

Journal of Materials Chemistry A

Accepted Manuscript



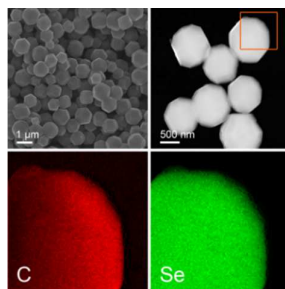
This is an *Accepted Manuscript*, which has been through the Royal Society of Chemistry peer review process and has been accepted for publication.

Accepted Manuscripts are published online shortly after acceptance, before technical editing, formatting and proof reading. Using this free service, authors can make their results available to the community, in citable form, before we publish the edited article. We will replace this *Accepted Manuscript* with the edited and formatted *Advance Article* as soon as it is available.

You can find more information about *Accepted Manuscripts* in the [Information for Authors](#).

Please note that technical editing may introduce minor changes to the text and/or graphics, which may alter content. The journal's standard [Terms & Conditions](#) and the [Ethical guidelines](#) still apply. In no event shall the Royal Society of Chemistry be held responsible for any errors or omissions in this *Accepted Manuscript* or any consequences arising from the use of any information it contains.

Table of Contents



A novel selenium-microporous carbon composite was synthesized and exhibited ultrastable cycling performance for rechargeable lithium-selenium batteries.

COMMUNICATION

Selenium-confined microporous carbon cathode for ultrastable lithium-selenium batteries

Cite this: DOI: 10.1039/x0xx00000x

Yunxia Liu, Ling Si, Xiaosi Zhou,* Xia Liu, Yan Xu, Jianchun Bao and Zhihui Dai*

Received 00th January 2012,

Accepted 00th January 2012

DOI: 10.1039/x0xx00000x

www.rsc.org/

A novel selenium-carbon composite has been fabricated by embedding selenium in metal-organic framework-derived microporous carbon polyhedrons. Such interconnected microporous carbon polyhedrons possess a large surface area and pore volume to effectively confine Se, and suppress the dissolution of polyselenides in electrolyte. This selenium-carbon composite shows ultrastable cycling performance when used as a cathode material for lithium-selenium batteries.

Rechargeable batteries with high energy density and long cycle life are essential for meeting the increasing need of energy storage.^{1–9} Recently, lithium-sulfur (Li-S) cells have attracted great attention due to their high theoretical gravimetric energy density of $\sim 2600 \text{ W h kg}^{-1}$, low cost, and nontoxicity.^{10–12} However, the commercialization of Li-S batteries has been seriously impeded by their poor cycle life. The rapid capacity decline during cycling is owing to three major issues, involving the dissolution of polysulfide intermediates in the electrolyte, large volume change ($\sim 80\%$), and the insulating nature of S.^{13,14} Various strategies have been proposed to overcome these issues, such as surface coating,^{15–17} new electrolytes and additives,^{18–21} and porous carbon matrixes.^{22–34} Although the significant progress has been realized, the practical application of Li-S cells is still hampered by the intrinsic drawbacks of S. Thereby, it is highly desirable to explore and develop novel high energy density cathode materials with enhanced cycling life.

Selenium has recently been considered as a promising cathode material because of its outstanding theoretical volumetric capacity density and high electronic conductivity.^{35–40} Despite Se possesses a lower gravimetric capacity (678 mA h g^{-1}) than that of sulfur (1672 mA h g^{-1}), its high density allows for a high volumetric capacity ($3253 \text{ mA h cm}^{-3}$ based on 4.82 g cm^{-3}), comparable to that of sulfur ($3467 \text{ mA h cm}^{-3}$ based on 2.07 g cm^{-3}).^{35,36} Furthermore, the electronic conductivity of Se ($1 \times 10^{-3} \text{ S m}^{-1}$) is much higher than that of sulfur ($5 \times 10^{-28} \text{ S m}^{-1}$), which facilitates the fast electrochemical reaction between Se and Li.³⁵ These

advantages of Se make it a prospective cathode material for fabricating high energy density batteries.

Recently reported results indicate that mesoporous carbon materials are desired hosts to greatly suppress the shuttle effect of Se cathodes. For instance, by impregnating Se in ordered mesoporous carbon (CMK-3) matrix, the Se/CMK-3 composite exhibits superior cycling performance and rate capability.³⁷ Another carbon material mesoporous carbon spheres have also been proved as a promising carbon host for Se.³⁸ These encouraging results show the features of mesoporous carbon materials, which might provide several advantages such as outstanding confinement capability, a large contact area with Se, and a short transport length for lithium ions.

Herein, we present the rational design and fabrication of a novel selenium-carbon composite by implanting Se in metal-organic framework-derived microporous carbon polyhedrons (MICP). Such MICP with interconnected microporous structures could maximize the features of porous carbon materials. Specifically, the interconnected micropores could effectively confine a relatively high amount of Se, restrict the outward diffusion of polyselenides, and buffer the large volume expansion during lithium insertion. When tested as a cathode material for Li-Se batteries, this composite exhibits ultralong cycle life and superior rate performance.

The microporous carbon polyhedrons are prepared using a polyhedral zeolitic imidazolate framework material ZIF-8 as the precursor. First, ZIF-8 polyhedrons were fabricated using a facile one-pot template-free approach reported previously.³² A subsequent annealing process under argon atmosphere at $1000 \text{ }^\circ\text{C}$ results in the carbonization of the ligand of ZIF-8 and the reduction of Zn^{2+} into metallic Zn that vaporizes at high temperature. The residual Zn can be easily washed by hydrochloric acid to produce MICP, which perfectly preserved the morphology and size of the ZIF-8 polyhedrons. These carbon particles with a uniform texture and no cracks or cavity could be clearly observed from the transmission electron microscope (TEM) image (Fig. 1a). The high-resolution TEM (HRTEM) image (Fig. 1b) on the edge of the carbon polyhedron obviously displays the existence of abundant micropores with sizes of $\sim 1.1 \text{ nm}$. Therefore, such a highly interconnected microporous carbon framework could serve as

an excellent matrix for Se loading. The MICP sample shows a quite high Brunauer–Emmett–Teller (BET) specific surface area of $890 \text{ m}^2 \text{ g}^{-1}$ and a large micropore volume of $0.474 \text{ cm}^3 \text{ g}^{-1}$ with a main pore size of $\sim 1.1 \text{ nm}$ (Fig. 2a), confirming its superior potential for Se impregnation.

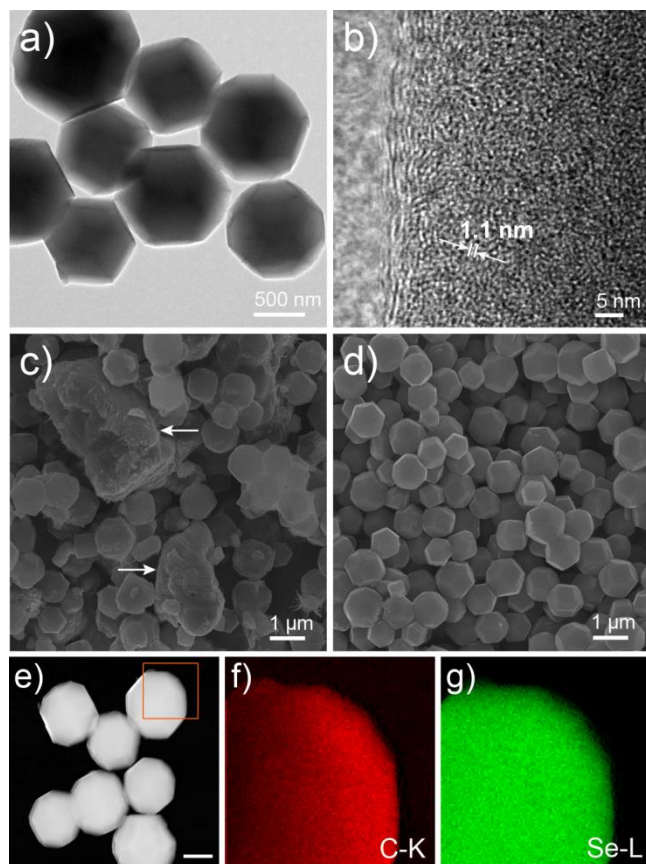


Fig. 1. (a, b) TEM and HRTEM images of MICP. (c) SEM image of Se-MICP. (d) SEM image of Se@MICP. (e) STEM image of Se@MICP, scale bar: 500 nm. (f, g) EDX elemental mapping based on the area marked in (e) for carbon and selenium, respectively.

Selenium encapsulation into MICP was carried out at $260 \text{ }^\circ\text{C}$ under vacuum, to promote the infusion of Se into the microporous carbon matrix and realize better impregnation of Se. After Se loading, the BET surface area of MICP decreases significantly (Fig. S1†), indicating the impregnation of Se into the micropores of MICP. The as-formed composite material, denoted as Se@MICP, was characterized by scanning electron microscope (SEM) images and HRTEM, which displayed similar morphology and structure compared to the pristine MICP sample and the disappearance of Se particles after the heating procedure (Fig. 1c, d, S2, 3†). The HRTEM image of Se@MICP (Fig. 3†) is almost the same as that of MICP, which is probably due to the transformation of cyclic Se_8 into chain-like Se_n , decreases the contrast of Se when compared with carbon under TEM measurement.^{37–39} Elemental mapping remarkably reveals the presence and uniform distribution of selenium in the carbon framework MICP. As shown in Fig. 1e–g, the similar distribution of selenium and carbon suggests the high affinity of the two components and the Se is well confined in the microporous carbon matrix.

Thermogravimetric analysis (TGA) of the Se@MICP composite in nitrogen flow displays a weight loss of

approximately 56% between 200 and $400 \text{ }^\circ\text{C}$, corresponding to the evaporation of Se from the composite material (Fig. 2b). Moreover, a slight weight loss of 5 % is found in the TGA curve of MICP. Thus the Se content in the Se@MICP sample was determined to be around 51 wt%. The powder X-ray diffraction (XRD) patterns of the physical mixture of Se and MICP (denoted as Se-MICP) and Se@MICP composite are illustrated in Fig. 2c. All of the diffraction peaks of crystallized Se disappear after heating, suggesting the phase transition has been occurred to selenium. The Raman spectra of Se, Se-MICP, and Se@MICP were measured to determine the structure of Se in Se@MICP (Fig. S4†). Compared with Se and Se-MICP, Se@MICP does display obvious change in Raman shift. After impregnation of Se into the micropores of MICP, the intensity of the characteristic peak of Se declines and its position blue shift to 255 cm^{-1} , which corresponds to the vibrations of amorphous Se consisting of chain-structured Se_n .^{37,38} Meanwhile, combined with the small amount of Se detected by X-ray photoelectron spectroscopy (XPS) on the surface of Se@MICP (5.1 at%, Fig. 2d), it could be concluded that most of amorphous Se is well confined in the micropores of MICP. The Se 3d XPS spectrum exhibits a broad peak at 59.0 eV, demonstrating that some Se near the surface of the Se@MICP was oxidized to SeO_2 (Fig. S5†).³⁹ The two large peaks at 56.2 eV (Se 3d_{3/2}) and 55.4 eV (Se 3d_{5/2}) confirm the existence of elemental Se.

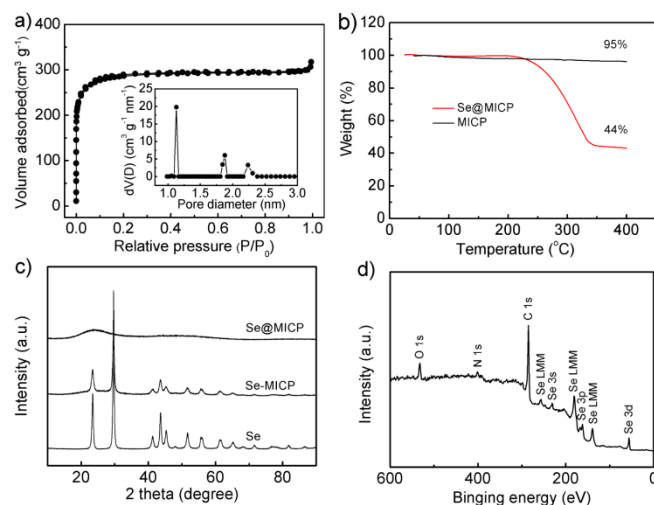


Fig. 2. (a) Nitrogen adsorption/desorption isotherms of MICP. Inset: Pore-size distribution plot calculated using the DFT method. (b) TGA curves of MICP and Se@MICP. (c) XRD patterns of Se, Se-MICP, and Se@MICP. (d) XPS survey scan of Se@MICP.

Fig. 3a shows cyclic voltammograms (CV) of the Se@MICP cathode for Li-Se batteries. The CV curves demonstrate only one pair of reversible redox peaks, suggesting that a single phase-change reaction has been taken place during the lithium uptake/release processes. In the first cycle, the cathodic peak and the anodic peak appear at 1.53 V and 2.02 V, respectively. Afterward, the anodic peak moves to a higher potential of 1.67 V, while the cathodic peak stays at 2.02 V. Hence, there is an electrochemical activation process during the first lithiation, and similar phenomena have been reported in other cathode materials.^{14,20,28} The stable anodic and cathodic peaks after the first cycle imply stable cycling performance of the Se@MICP composite. Fig. 3b shows the charge/discharge profiles for

different cycles within a voltage range of 1.5–3.0 V, which were in good agreement with the above CV results.

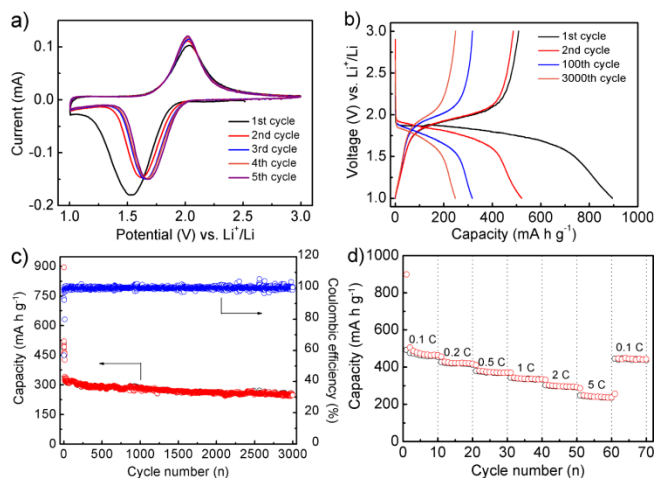


Fig. 3. (a) CV curves of the first five cycles of Se@MICP. (b) Galvanostatic charge/discharge profiles for different cycles of Se@MICP. (c) Cycling performance and Coulombic efficiency of Se@MICP; the first ten cycles are at 0.1 C, and the remaining cycles are at 1 C. (d) Rate performance of Se@MICP.

Fig. 3c displays the cycling performance of the Se@MICP composite. At a current density of 0.1 C (67.8 mA g^{-1}), the initial charge and discharge capacities of the Se@MICP composite are 508 and 895 mA h g^{-1} (based on the mass of Se, same below), respectively. The irreversible capacity loss is generally attributed to the electrolyte decomposition on the surface of the carbon matrix MICP. However, the irreversible capacity of Se-MICP is not as large as that of Se@MICP. This is probably due to the surface of MICP covered with Se, as shown in Fig 1c, thus impeding the electrolyte decomposition on the surface of MICP. When the current density increases to 1 C after the first ten cycles at 0.1 C, the Se@MICP composite delivers a discharge capacity of 341 mA h g^{-1} . Even after 3000 cycles, a capacity of 249 mA h g^{-1} is retained. The superior capacity retention of the Se@MICP composite under high rate can probably be attributed to the unique porous structure of the carbon matrix, in which the highly interconnected microporous network functions as a smart carbon host for Se encapsulation. During the repeated charge/discharge processes of the Se@MICP electrode, the dissolution of polyselenides and the loss of Se were considerably limited by the interconnected micropores as proved by the relatively high Coulombic efficiency (Fig. 3c). Besides, the flexible character of the carbon host could effectively mitigate the mechanical stress caused by the large volume change upon cycling. To further demonstrate the structural advantages of Se@MICP, Se-MICP was also evaluated as cathode for comparison. After 1000 cycles, the discharge capacity of Se-MICP is only 48 mA h g^{-1} (Fig. S6†), while Se@MICP exhibits a capacity of 283 mA h g^{-1} . The rate capability of the composite is displayed in Fig. 3d. The discharge capacity gradually decreases as the current rate increases from 0.1 C to 5 C. A satisfactory capacity of 241 mA h g^{-1} is achieved for Se@MICP at 5 C (3390 mA h g^{-1}), comparable to the reported values,^{37,38} and the composite recovers most of the capacity when the current density return to 0.1 C. The superior rate performance of the Se@MICP composite is likely due to the boosted kinetic parameters including electronic/ionic transportation in the carbon matrix

MICP. Additionally, as the current density increases from 0.1 C to 5 C, the charge-discharge profiles display analogous shapes, with increasing of the voltage difference, which is due to polarization loss and mechanical energy dissipation during battery cycling (Fig. S7†).

The ultrastable cycling performance of Se@MICP is believed to be correlated to the unique structure of the composite. Thus, the morphology and interior structure of Se@MICP after 3000 cycles battery test are surveyed by scanning transmission electron microscope (STEM) and energy dispersive X-ray spectroscopy (EDX) elemental mapping techniques (Fig. 4). Compared to Fig. 1e–g, no obvious morphology change could be observed after 3000 cycles (Fig. 4a, c, d), suggesting this robust microporous carbon can effectively buffer the large volume variation of Se during lithium insertion/extraction. Besides, the EDX elemental mapping results show that Se is still uniformly distributed in the microporous carbon matrix even after 3000 cycles (Fig. 4b–d), further verifying the strong confinement ability of MICP on polyselenides. Moreover, we performed electrochemical impedance spectroscopy measurements of the Se@MICP electrode before test and after 5 cycles (Fig. S8†). The impedance decrease upon cycling can be probably ascribed to the delayed infiltration of electrolyte into the composite, which is consistent with the CV results.

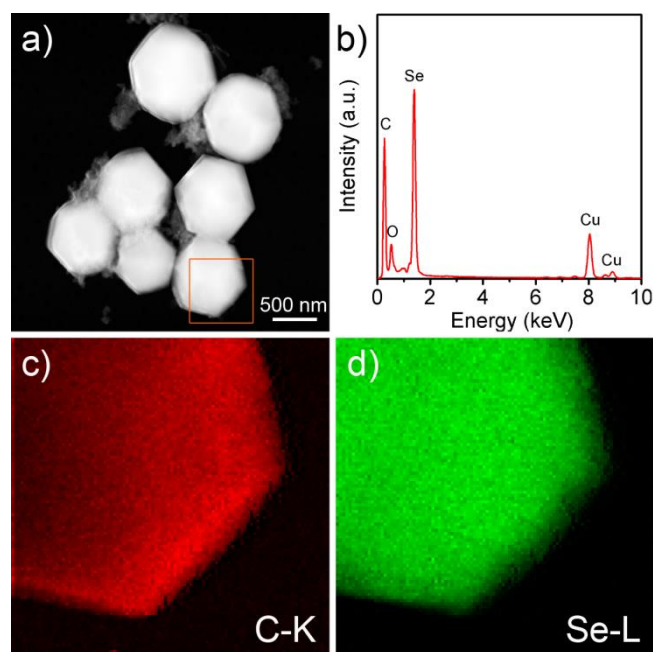


Fig. 4. (a, b) STEM image and EDX spectrum of Se@MICP after cycling test. (c, d) Corresponding C and Se elemental mapping based on the area displayed in (a).

Conclusions

In summary, we have impregnated Se in microporous carbon polyhedrons through a facile melt-diffusion approach. Such interconnected microporous carbon polyhedrons bring about a large surface area and pore volume to effectively confine Se, and suppress the dissolution of polyselenides in electrolyte at the same time. Additionally, the transport for electrons and Li ions and the ability to withstand volume variation are also enhanced, resulting from the unique microporous structure of

the carbon host. As a consequence, when used as a cathode material for Li-Se batteries, the Se@MICP composite give superior electrochemical performance in terms of specific capacity and cycling stability as well as rate capability.

Acknowledgements

This work was supported by the National Natural Science Foundation of China (Grant Nos. 21175069 and 21171096), the Scientific Research Foundation for Advanced Talents of Nanjing Normal University (2014103XGQ0073), the financial support from the Priority Academic Program Development of Jiangsu Higher Education Institutions, and the Program of Jiangsu Collaborative Innovation Center of Biomedical Functional Materials.

Notes and references

Jiangsu Key Laboratory of Biofunctional Materials, School of Chemistry and Material Science, Nanjing Normal University, Nanjing 210023, P. R. China. E-mail: zhouxiaosi@njnu.edu.cn; daizhihui@njnu.edu.cn

† Electronic Supplementary Information (ESI) available: Experimental details, and additional SEM image, HRTEM image, Raman spectra, cycling performance, charge/discharge profiles, and Nyquist plots. See DOI: 10.1039/c000000x/

- 1 Y.-K. Sun, S.-T. Myung, B.-C. Park, J. Prakash, I. Belharouak and K. Amine, *Nat. Mater.*, 2009, **8**, 320–324.
- 2 M. Armand and J.-M. Tarascon, *Nature*, 2008, **451**, 652–657.
- 3 J. B. Goodenough and Y. Kim, *Chem. Mater.*, 2010, **22**, 587–603.
- 4 Z. Zhu, S. Wang, J. Du, Q. Jin, T. Zhang, F. Cheng and J. Chen, *Nano Lett.*, 2014, **14**, 153–157.
- 5 L. Shen, E. Uchaker, X. Zhang and G. Cao, *Adv. Mater.*, 2012, **24**, 6502–6506.
- 6 C. Zhu, X. K. Mu, P. A. van Aken, Y. Yu and J. Maier, *Angew. Chem. Int. Ed.*, 2014, **53**, 2152–2156.
- 7 X. Meng, X.-Q. Yang and X. Sun, *Adv. Mater.*, 2012, **24**, 3589–3615.
- 8 T. Zhang and H. Zhou, *Nat. Commun.*, 2013, **4**, 1817.
- 9 X. Zhou, L.-J. Wan and Y.-G. Guo, *Adv. Mater.*, 2013, **25**, 2151–2157.
- 10 A. Manthiram, Y. Fu and Y.-S. Su, *Acc. Chem. Res.*, 2013, **46**, 1125–1134.
- 11 X. Ji and L. F. Nazar, *J. Mater. Chem.*, 2010, **20**, 9821–9826.
- 12 P. G. Bruce, S. A. Freunberger, L. J. Hardwick and J.-M. Tarascon, *Nat. Mater.*, 2012, **11**, 19–29.
- 13 Y. V. Mikhaylik and J. R. Akridge, *J. Electrochem. Soc.*, 2004, **151**, A1969–A1976.
- 14 G.-C. Li, G.-R. Li, S.-H. Ye and X.-P. Gao, *Adv. Energy Mater.*, 2012, **2**, 1238–1245.
- 15 R. Chen, T. Zhao, J. Lu, F. Wu, L. Li, J. Chen, G. Tan, Y. Ye and K. Amine, *Nano Lett.*, 2013, **13**, 4642–4649.
- 16 H. Wang, Y. Yang, Y. Liang, J. T. Robinson, Y. Li, A. Jackson, Y. Cui and H. Dai, *Nano Lett.*, 2011, **11**, 2644–2647.
- 17 G. Zhou, L.-C. Yin, D.-W. Wang, L. Li, S. Pei, I. R. Gentle, F. Li and H.-M. Cheng, *ACS Nano*, 2013, **7**, 5367–5375.
- 18 D.-R. Chang, S.-H. Lee, S.-W. Kim and H.-T. Kim, *J. Power Sources*, 2002, **112**, 452–460.
- 19 J. Wang, S. Y. Chew, Z.W. Zhao, S. Ashraf, D. Wexler, J. Chen, S. H. Ng, S. L. Chou and H. K. Liu, *Carbon*, 2008, **46**, 229–235.
- 20 L. Ji, M. Rao, H. Zheng, L. Zhang, Y. Li, W. Duan, J. Guo, E. J. Cairns and Y. Zhang, *J. Am. Chem. Soc.*, 2011, **133**, 18522–18525.
- 21 L. Suo, Y.-S. Hu, H. Li, M. Armand and L. Chen, *Nat. Commun.*, 2013, **4**, 1481.
- 22 X. Ji, K. T. Lee and L. F. Nazar, *Nat. Mater.*, 2009, **8**, 500–506.
- 23 C. Liang, N. J. Dudney and J. Y. Howe, *Chem. Mater.*, 2009, **21**, 4724–4730.
- 24 S.-R. Chen, Y.-P. Zhai, G.-L. Xu, Y.-X. Jiang, D.-Y. Zhao, J.-T. Li, L. Huang and S.-G. Sun, *Electrochim. Acta*, 2011, **56**, 9549–9555.
- 25 N. Jayaprakash, J. Shen, S. S. Moganty, A. Corona and L. A. Archer, *Angew. Chem. Int. Ed.*, 2011, **50**, 5904–5908.
- 26 J. Guo, Y. Xu and C. Wang, *Nano Lett.*, 2011, **11**, 4288–4294.
- 27 R. Elazari, G. Salitra, A. Garsuch, A. Panchenko and D. Aurbach, *Adv. Mater.*, 2011, **23**, 5641–5644.
- 28 L. Xiao, Y. Cao, J. Xiao, B. Schwenzer, M. H. Engelhard, L. V. Saraf, Z. Nie, G. J. Exarhos and J. Liu, *Adv. Mater.*, 2012, **24**, 1176–1181.
- 29 C. Zhang, H. B. Wu, C. Yuan, Z. Guo and X. W. Lou, *Angew. Chem. Int. Ed.*, 2012, **51**, 9592–9595.
- 30 S. Xin, L. Gu, N.-H. Zhao, Y.-X. Yin, L.-J. Zhou, Y.-G. Guo and L.-J. Wan, *J. Am. Chem. Soc.*, 2012, **134**, 18510–18513.
- 31 S. Zheng, Y. Chen, Y. Xu, F. Yi, Y. Zhu, Y. Liu, J. Yang and C. Wang, *ACS Nano*, 2013, **7**, 10995–11003.
- 32 H. B. Wu, S. Wei, L. Zhang, R. Xu, H. H. Hng and X. W. Lou, *Chem. Eur. J.*, 2013, **19**, 10804–10808.
- 33 J. Kim, D.-J. Lee, H.-G. Jung, Y.-K. Sun, J. Hassoun and B. Scrosati, *Adv. Funct. Mater.*, 2013, **23**, 1076–1080.
- 34 H. Yao, G. Zheng, P.-C. Hsu, D. Kong, J. J. Cha, W. Li, Z. W. Seh, M. T. McDowell, K. Yan, Z. Liang, V. K. Narasimhan and Y. Cui, *Nat. Commun.*, 2014, **5**, 3943.
- 35 A. Abouimrane, D. Dambournet, K. W. Chapman, P. J. Chupas, W. Weng and K. Amine, *J. Am. Chem. Soc.*, 2012, **134**, 4505–4508.
- 36 L. Liu, Y. Hou, X. Wu, S. Xiao, Z. Chang, Y. Yang and Y. Wu, *Chem. Commun.*, 2013, **49**, 11515–11517.
- 37 C.-P. Yang, S. Xin, Y.-X. Yin, H. Ye, J. Zhang and Y.-G. Guo, *Angew. Chem. Int. Ed.*, 2013, **52**, 8363–8367.
- 38 C. Luo, Y. Xu, Y. Zhu, Y. Liu, S. Zheng, Y. Liu, A. Langrock and C. Wang, *ACS Nano*, 2013, **7**, 8003–8010.
- 39 H. Ye, Y.-X. Yin, S.-F. Zhang and Y.-G. Guo, *J. Mater. Chem. A*, 2014, **2**, 13293–13298.
- 40 Y. Cui, A. Abouimrane, C.-J. Sun, Y. Ren and K. Amine, *Chem. Commun.*, 2014, **50**, 5576–5579.